A Predefined Time Fast Terminal Sliding Mode Predictive Speed Control for PMSM Drives

Delin Kong, *Graduate Student Member, IEEE*, Haiwei Cai, *Member, IEEE*, and Wenkai Zeng, *Student Member, IEEE*

***Abstract*—This article proposes an improved predefined time sliding mode predictive control strategy for surface-mounted permanent magnet synchronous motor to achieve superior antidisturbance capability and tracking performance. Compared to the conventional predefined time sliding mode surface (PTSLMS), a linear term is introduced to enhance the convergence rate of system states. A more broadly applicable formulation of the PTSLMS is presented. Then, a cost function is provided to make the one-step forward prediction of the sliding mode surface approach the target value. The lumped disturbances from load torque and uncertainties are estimated and compensated by an enhanced predefined time disturbance observer. Simulations and experiments are carried out to verify the effectiveness of the proposed method in dynamic response performance and antidisturbance capability.**

***Index Terms*—Convergence rate, permanent magnet synchronous motor (PMSM), predefined time, sliding mode predictive control (SMPC), speed regulation.**

I. Introduction

PERMANENT magnet synchronous motors (PMSMs), have been extensively applied in machine tool processing, servo-driven robots and new energy industries for their inherit advantages, such as high efficiency, high-power density and small installation volume [1], [2]. PI control, as a commonly algorithm for PMSM speed control, is limited by the nonlinear modeling of PMSM and cannot satisfy some specific requirements for the dynamic response performance and antidisturbance capability [3]. Thereby, many nonlinear algorithms emerged, such as model predictive control (MPC), sliding mode control (SMC) and adaptive control, etc.

MPC has caught the attention of scholars for the evolution of the digital technology and its simplicity in dealing with nonlinear problems [4]. MPC can be effectively applied to nonlinear systems by utilizing explicit models of PMSM and minimizing a cost function over a finite prediction horizon. However, this approach inherently implies that the control performance of MPC is highly dependent on the accuracy of the system model. In addition, MPC is sensitive to external disturbances, which has been hot issues in current research [5], [6]. Hence, a continuous control set MPC speed control method with reduced-order increment model of SPMSM is proposed, which naturally includes integrators. The experimental results confirm that the proposed method effectively eliminates steady-state errors induced by both parameter variations and external disturbances. However, the enhancement of antidisturbance capability remains limited and requires further improvement. Additionally, a short prediction horizon is utilized to balance steady-state performance and dynamic response [7].

To improve the robustness to parameter variations, motor parameters of different operating conditions are identified offline as presented in [8]. However, it is difficult to identify the parameters of all operating conditions and enhance the resistance to external disturbances. Least squares (LSs) method can estimate parameters according to the measurements recorded online and update the model at the present moment to improve the control performance [9]. Recursive LS (RLS) method can estimate and update system models online uninterruptedly, which reduces the dependence of the MPC on the disturbances of parameter variations [10], [11], [12]. Model reference adaptive system method has been wildly applied in parameters identification for less computational load compared to the LS and RLS [13]. However, the impact of external disturbances on MPC has not been taken into account in these methods.

Disturbance observers (DOs) can estimate and compensate systems disturbances, including parameter variations and external disturbances, which significantly improves systems antidisturbance capability [14]. To mitigate the sensitivity of MPC to external disturbances, a dual second-order sliding-mode disturbance observer is proposed for estimating lumped disturbances. The estimated disturbances are then integrated into deadbeat predictive direct speed control to compensate for significant disturbances and model uncertainties in PMSM. The effectiveness of dynamic response and disturbance rejection performance is verified by simulations. However, the stabilization time of the observer is disregarded [15]. A novel sliding mode exponential reaching law-based DO is utilized to improve the robustness of the PMSM deadbeat predictive current control. The results of simulations and experiments indicate the effectiveness of the proposed approach. The proposed DO can achieve finite time stabilization. However, the stabilization and convergence

Received 11 October 2024; revised 31 January 2025; accepted 15 February 2025. Date of publication 21 February 2025; date of current version 14 April 2025. This work was supported in part by the Aeronautical Science Foundation of China under Grant 2024M067069001 and in part by the SEU Innovation Capability Enhancement Plan for Doctoral Students under Grant CXJH_SEU_25159. Recommended for publication by Associate Editor R. Kennel. *(Corresponding author: Haiwei Cai.)*

The authors are with the School of Electrical Engineering, Southeast University, Nanjing 210096, China (e-mail: 230238814@seu.edu.cn; haiweicai@seu.edu.cn; 220213079@seu.edu.cn).

Color versions of one or more figures in this article are available at https://doi.org/10.1109/TPEL.2025.3544281.

Digital Object Identifier 10.1109/TPEL.2025.3544281

time depend on the initial state of the system [16]. Similarly, the stabilization time of the DO in [17] is also affected by the initial state of the system. In [18], a second-order fixed time convergence sliding mode observer (FTSMO) is presented to enhance the robustness of the model-free predictive current control of PMSM. Although the stabilization time of FTSMO can be less than a maximum value for any initial state of systems, it still cannot be predefined and is often desired to be shorter. Therefore, a DO that can stabilize within a faster and predefined time needs to be researched.

By exploiting the robustness of SMC [19], [20], [21], sliding mode predictive control (SMPC) has been extensively studied, which integrates SMC into MPC. SMPC differs from MPC in that the cost function is defined as the deviation between the one-step forward prediction value and the target value of the sliding mode surface. The optimal control output is then obtained by minimizing the cost function, consistent with the approach used in MPC. An SMPC based on linear sliding mode surface (LSMS) is proposed for the boiler-turbine system with uncertainties [22]. Although the simulation results indicate that the proposed strategy enhances the antidisturbance capability, the system is asymptotically stable. To enhance the antidisturbance capability of the MPC for the SPMSM speed regulation, an SMPC with an LSMS is proposed in [17]. The same PI current controllers are designed for both SMPC and MPC. The results show that the proposed method can effectively improve the robustness of MPC. However, since the sliding mode surface is linear, the system is asymptotically stable.

Kang et al. [23] proposed an SMPC utilizing fast terminal sliding mode surface (FTSLMS) for a parallel micropositioning piezostage to achieve faster convergence of the sliding mode surface and the system states. This approach improves the dynamic response performance and the robustness of MPC, but the convergence of the system states is still affected by the initial state of the system.

The issue of the system states convergence performance being dependent on the initial state of the system has been addressed in several studies on SMC. For example, fixed time SMC is proposed, which can realize the fixed time convergence of the system regardless of the initial state of the system [24], [25]. However, the system states convergence time cannot be predefined. A predefined time SMC is developed and validated on a space triangle tethered formation system. The system states can converge in a predefined time [26], but the convergence rate still needs to be improved. To achieve better dynamic response performance, a linear term is introduced into traditional predefined time frameworks in [27], which not only realizes the predefined time convergence but also increases the convergence rate of the system states.

However, there is little research on the application of predefined time SMPC theory to PMSM. In [28], a predefined time sliding mode predictive method for SPMSM speed control is proposed. The robustness and tracking performance are verified to be enhanced by experiments, but it is generally desired that the system converges as fast as possible. Therefore, a linear item is introduced into traditional predefined time SMPC for SPMSM speed control to accelerate the system convergence rate in this article. The existing predefined time theory applied in SMC of synchronizing chaotic systems [27], including linear item, is adjusted by the predefined time parameter for the output control gain. Since the introduction of a linear term, the system is prone to jitter when the predefined time is small, especially for some small inertia PMSM speed control. Meanwhile, there is potential to further improve the dynamic response performance and robustness of the system.

Considering the shortcomings of [27], a predefined time fast terminal SMPC method based on a predefined time DO is proposed for PMSM speed control in this article. First, a linear term and adjustment parameters are introduced into the traditional predefined time sliding mode surface (PTSLMS) to speed up the system convergence rate and facilitate the adjustment of the control output gain. A predefined time FTSLMS (PTFTSLMS) with broader applicability is thus established. Then, the stability analysis is presented, and a DO based on the improved predefined time reaching law is designed for observing and compensating for the lump disturbances of parameter variations and external disturbances. Next, a cost function is defined by the error between the sliding mode surface of one-step forward prediction and its target value. Finally, the control output gain of the speed control is obtained by minimizing the cost function.

The rest of this article is organized as follows. Section II introduces the mathematical model of SPMSM and preliminaries. The proposed predefined time fast terminal SMPC and predefined time DO are shown in Section III. Simulation and experimental comparisons are carried out in Section IV. Finally, Section V concludes the article.

II. Mathematical Model and Preliminaries

A. Mathematical Model of SPMSM

The general mathematical model of SPMSM can be expressed as

$$\begin{cases} J\frac{d\omega_m}{dt} = T_e - T_L - b\omega_m \\ T_e = \frac{3}{2}pi_q\psi_f \end{cases} \tag{1}$$

where J is rotational inertia, T_e is electromagnetic torque, T_L is the load torque, ω_m is the rotor speed in rad/s, b is coefficient of viscous friction, p is number of magnetic poles, ψ_f is permanent magnet flux linkage, R_s is stator resistance, and i_d, i_q are stator current magnitude dq components.

In fact, the parameters of SPMSM systems are affected by parameter perturbation, system uncertainty, and external disturbance. These parameters can be described as

$$\begin{cases} J = J_0 + \Delta J \\ \psi_f = \psi_{f0} + \Delta\psi_f \end{cases} \tag{2}$$

where J_0 and ψ_{f0} represent the nominal values, ΔJ and $\Delta\psi_f$ denote the uncertainty values. SPMSM systems typically consist of an inner loop (speed loop) and outer loop (current loop). The reference for the current control $(i_{d\text{ref}})$ on the d-axis component is 0A and the output of the speed control determines the reference for the q-axis component $(i_{q\text{ref}})$.

When $i_{dref} = 0$ A, the reference of the mechanical equation can be derived as (3) from (1) (2)

$$\dot{\omega}_m = ai_q - d_l \tag{3}$$

where $d_l = 3p(\Delta\psi_f J_0 - \Delta J\psi_{f0})/2J_0\Delta J + b\omega_m/J + T_L/J$ is the lumped disturbance, including parameter perturbation, system uncertainty, and external disturbance, and $a = 3p\psi_{f0}/2J_0$.

The speed tracking error is defined as

$$\begin{cases} e_1 = \omega_r - \omega_m \\ e_2 = \dot{\omega}_r - \dot{\omega}_m \end{cases} \tag{4}$$

where e_1 is the speed tracking error, e_2 is the derivative of e_1, and ω_r is the speed reference in rad/s.

By combining (3) and (4), (5) is derived

$$\begin{cases} \dot{e}_1 = e_2 \\ \dot{e}_2 = -au + \dot{d}_l \end{cases} \tag{5}$$

where u is the output of the speed loop.

B. Preliminaries

A nonlinear system is defined as

$$\dot{x} = f(x), x(0) = x_0 \tag{6}$$

where $x \in R^n$ represents the system states, and $f(x)$ is known.

Definition 3.1 [29]: System (6) is called predefined time stable if it can achieve global stability within a predefined time T_c, where the stability time $T_x(x_0) \le T_c, \forall x_0 \in R^n$.

Lemma 1 [27]: For the system (6), if there exists a Lyapunov function V satisfying

$$V \le -\frac{1}{T_c}\frac{2}{\alpha}\left(2V + V^{1-\frac{\alpha}{2}} + V^{1+\frac{\alpha}{2}}\right). \tag{7}$$

Then, the system (6) is called predefined time stable, where $Tc > 0$ is the predefined time and $0 < \alpha < 1$.

III. Predefined Time Fast Terminal Sliding Mode Predictive Control and Improved Predefined Time Disturbance Observer

A. Predefined Time Fast Terminal Sliding Mode Predictive Control (PTFTSMPC)

1) Predefined Time Fast Terminal Sliding Mode Surface: To suppress the potential jitter caused by the introduction of linear terms which aims to accelerate the convergence rate and extend the application range of the existing predefined time theorem in [27], a PTFTSLMS is introduced. This enables its application to SPMSM speed control. The general form of PTFTSLMS is shown as

$$\begin{cases} s_\omega = e_2 + \frac{B}{T}\left(\chi_1 \mathrm{sgn}^{1-\nu}(e_1) + \chi_3 e_1 + \chi_2 \mathrm{sgn}^{1+\nu}(e_1)\right) \\ B = \begin{cases} \frac{1}{\nu\sqrt{\chi_1\chi_2}}, \chi_3 = 2\sqrt{\chi_1\chi_2} \\ \frac{1}{\nu\chi_2\varsigma^{\frac{1}{2}}}\left[\frac{\pi}{2} - \arctan\left(\varsigma^{-\frac{1}{2}}\frac{\chi_3}{2\chi_2}\right)\right], \chi_3 > 2\sqrt{\chi_1\chi_2} \end{cases} \end{cases} \tag{8}$$

where s_ω is the sliding mode surface, χ_1, χ_2, $\chi_3 > 0$, $0 < \nu < 1$, $\chi_3 \le 2\sqrt{\chi_1\chi_2}$, $\mathrm{sgn}^{1-\nu}(e_1) = |e_1|^{1-\nu}\mathrm{sign}(e_1)$, and $\mathrm{sgn}^{1+\nu}(e_1) = |e_1|^{1+\nu}\mathrm{sign}(e_1)$. Here, T is the system states convergence time, $\varsigma = \frac{\chi_1}{\chi_2} - (\frac{\chi_3}{2\chi_2})^2$, $\wp(e_1) = e_1^\nu + \frac{\chi_3}{2\chi_2}$. When $B = \frac{1}{\nu\sqrt{\chi_1\chi_2}}$ and $\chi_1 = \chi_2 = 1$, the design of (8) is consistent with that in [27].

When the sliding mode face $s_\omega = 0$, (9) can be derived

$$e_2 = -\frac{B}{T}\left(\chi_1 \mathrm{sgn}^{1-\nu}(e_1) + \chi_3 e_1 + \chi_2 \mathrm{sgn}^{1+\nu}(e_1)\right). \tag{9}$$

2) Convergence Time: The time for the system states to converge from the initial value $e_1(0)$ to zero is defined as t, and t can be derived by solving (9)

$$\int_0^t dt = \int_0^t -\frac{Tde_1}{B\left(\chi_1 \mathrm{sgn}^{1-\nu}(e_1) + \chi_3 e_1 + \chi_2 \mathrm{sgn}^{1+\nu}(e_1)\right)}. \tag{10}$$

Then t can be expressed as

$$t = \int_{e_1(0)}^{e_1(t)} -\frac{Tdx_1^\nu}{B\nu\chi_2\left[\left(e_1^\nu + \frac{\chi_3}{2\chi_2}\right)^2 + \frac{\chi_1}{\chi_2} - \left(\frac{\chi_3}{2\chi_2}\right)^2\right]}. \tag{11}$$

Case $\frac{\chi_1}{\chi_2} - (\frac{\chi_3}{2\chi_2})^2 = 0, \chi_3 = 2\sqrt{\chi_1\chi_2}$, it can be obtained that

$$\begin{aligned} t &= \int_{e_1(0)}^{e_1(t)} -\frac{Tde_1^\nu}{B\nu\chi_2\left[\left(e_1^\nu + \sqrt{\frac{\chi_1}{\chi_2}}\right)^2\right]} \\ &= \frac{T}{B\nu\chi_2}\frac{1}{e_1^\nu + \sqrt{\frac{\chi_1}{\chi_2}}}\Bigg|_{e_1(0)}^{e_1(t)} \\ &\le \frac{T}{B\nu\sqrt{\chi_1\chi_2}}. \end{aligned} \tag{12}$$

Substituting (8) into (12), it can be obtained that $t \le T$. Thus, the system state e_1 can converge within a predefined time T. The (13) can be derived as

$$s_\omega = e_2 + \chi_1 \mathrm{sgn}^{1-\nu}(e_1) + 2\sqrt{\chi_1\chi_2}e_1 + \chi_2 \mathrm{sgn}^{1+\nu}(e_1). \tag{13}$$

Case $\frac{\chi_1}{\chi_2} - (\frac{\chi_3}{2\chi_2})^2 > 0,\ \chi_3 > 2\sqrt{\chi_1\chi_2}$, it yields that

$$\begin{aligned} t &= \int_{e_1(0)}^{e_1(t)} -\frac{Td\left[\varsigma^{-\frac{1}{2}}\wp(e_1)\right]}{B\nu\chi_2\varsigma^{\frac{1}{2}}\left[\varsigma^{-\frac{1}{2}}\wp^2(e_1) + 1\right]} \\ &= \frac{T}{-B\nu\chi_2\varsigma^{\frac{1}{2}}}\arctan\left[\varsigma^{-\frac{1}{2}}\wp(e_1)\right]\Bigg|_{e_1(0)}^{e_1(t)} \\ &\le \frac{T}{B\nu\chi_2\varsigma^{\frac{1}{2}}}\left[\frac{\pi}{2} - \arctan\left(\varsigma^{-\frac{1}{2}}\frac{\chi_3}{2\chi_2}\right)\right]. \end{aligned} \tag{14}$$

By substituting (8) into (14), it can be derived that $t \le T$, and the system state e_1 can converge from initial state $e_1(0)$ to zero within a predefined time T. Equation (15) can then be obtained as

$$\begin{aligned} s_\omega = e_2 + \frac{\frac{\pi}{2} - \arctan\left(\varsigma^{-\frac{1}{2}}\frac{\chi_3}{2\chi_2}\right)}{T\nu\chi_2\varsigma^{\frac{1}{2}}}\left(\chi_1 \mathrm{sgn}^{1-\nu}(e_1)\right. \\ \left. + \chi_3 e_1 + \chi_2 \mathrm{sgn}^{1+\nu}(e_1)\right). \end{aligned} \tag{15}$$

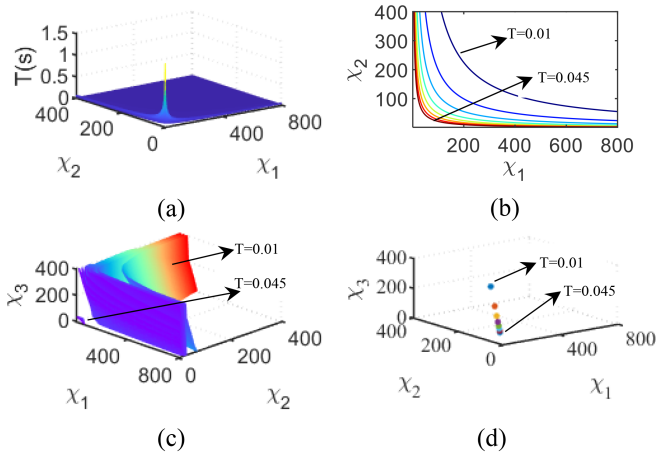

Fig. 1. Relationship between T and the adjustment parameters of $\mathrm{sgn}^{1-\nu}(e_1)$, $\mathrm{sgn}^{1+\nu}(e_1)$, and e_1. (a) $\chi_3 = 2\sqrt{\chi_1\chi_2}$. (b) $\chi_3 = 2\sqrt{\chi_1\chi_2}$. (c) $\chi_3 > 2\sqrt{\chi_1\chi_2}$. (d) $\chi_3 = 2\sqrt{\chi_1\chi_2} = 1$.

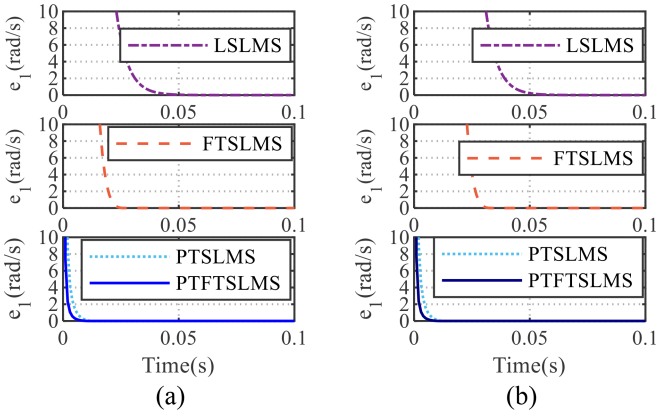

Fig. 2. System states convergence rate comparison between LSLMS, FTSLMS, PTSLMS, and the proposal PTFTSLMS. (a) $e_1(0) = 1000$. (b) $e_1(0) = 5000$.

When $\frac{B}{T} = 1$, χ_1, χ_2, χ_3 are the direct tuning factors of each component in the proposed PTFTSLMS. For the convenience of parameter selection, the $\frac{B}{T}$ is set to 1, and then χ_1, χ_2, and χ_3 can be obtained at different values of T. A smaller value of T may lead to system jitter. The relationships between the system states settling time and χ_1, χ_2, and χ_3 are shown in Fig. 1(a), (b), and (c).

When $\frac{\chi_1}{\chi_2} - \left(\frac{\chi_3}{2\chi_2}\right)^2 = 0$ and $\chi_3 = 2\sqrt{\chi_1\chi_2}$, the selection of χ_1, χ_2 and χ_3 is performed on a curve at a predefined time. When $\frac{\chi_1}{\chi_2} - \left(\frac{\chi_3}{2\chi_2}\right)^2 > 0$ and $\chi_3 > 2\sqrt{\chi_1\chi_2}$, the selection of χ_1, χ_2, and χ_3 is performed on a surface at a predefined time. The final parameters T, χ_1, χ_2, and χ_3 are obtained by scanning the parameter groupings in Fig. 1(a), (b), and (c).

The factor parameters for the provided PTSLMS in [27] correspond to a fixed point at a predefined convergence time without the adjustment of χ_1, χ_2, χ_3, as shown in Fig. 1(d). In contrast, this may reduce the parameter tuning task but limit the adjustment of the control gain. Parameter tunability is reduced at the same predefined time, which will likely affect the convergence performance. Moreover, as the time parameter decreases, it is more prone to cause the system jitter at the same predefined time.

Compared with the predefined time theorem in [27], PTFTSLMS shows better parameter tuning capability and a wider range of the control gain adjustments, which is meaningful for applications in small inertia systems. The proposed PTFTSLMS, lLSMS [17], FTSLMS [30] and PTSLMS [27] are compared in Fig. 2. Obviously, the proposal PTFTSLMS can converge faster compared to the others.

3) Stability Analysis: When $s_\omega \to 0$, the system states will slide on the sliding mode surface, and (9) is achieved. A Lyapunov function is chosen as $V = \frac{1}{2}e_1^2$, and the derivative of V can be expressed as

$$\begin{aligned}\dot{V} &= e_1\dot{e}_1 \\ &= e_1 e_2 \\ &= -\frac{B}{T}\left(\chi_1|e_1|^{2-\nu} + \chi_3 e_1^2 + \chi_2|e_1|^{2+\nu}\right) \le 0. \end{aligned} \tag{16}$$

When $B = \frac{1}{\nu\sqrt{\chi_1\chi_2}}$ and $\chi_1 = \chi_2 = 1$, the (16) is the same as *Lamma 1*. Equation (16) indicates that the system can be globally stable, and it can be simplified as

$$\begin{aligned}\dot{V} &= \frac{-B}{T}\left(2^{1-\frac{\nu}{2}}\chi_1\left(\frac{1}{2}e_1^2\right)^{1-\frac{\nu}{2}} + 2\chi_3\left(\frac{1}{2}e_1^2\right)\right. \\ &\quad \left. + 2^{1+\frac{\nu}{2}}\chi_2\left(\frac{1}{2}e_1^2\right)^{1+\frac{\nu}{2}}\right) \\ &= \frac{-B}{T}\left(2^{1-\frac{\nu}{2}}\chi_1 V^{1-\frac{\nu}{2}} + 2\chi_3 V + 2^{1+\frac{\nu}{2}}\chi_2 V^{1+\frac{\nu}{2}}\right). \end{aligned} \tag{17}$$

Then, the time for system stabilization t_V can be derived by solving (17)

$$\begin{aligned} t_V &= \int_{V(0)}^{V(t_V)} -\frac{TdV}{B\left(2^{1-\frac{\nu}{2}}\chi_1 V^{1-\frac{\nu}{2}} + 2\chi_3 V + 2^{1+\frac{\nu}{2}}\chi_2 V^{1+\frac{\nu}{2}}\right)} \\ &= \int_{V(0)}^{V(t_V)} -\frac{Td(2V)^\nu}{B\left(\chi_1 + \chi_3(2V)^{\frac{\nu}{2}} + \chi_2(2V)^\nu\right)}. \end{aligned} \tag{18}$$

Case $\frac{\chi_1}{\chi_2} - \left(\frac{\chi_3}{2\chi_2}\right)^2 = 0, \chi_3 = 2\sqrt{\chi_1\chi_2}$, the (18) can be expressed as

$$\begin{aligned} t_V &= \int_{V(0)}^{V(t_V)} -\frac{T\nu\sqrt{\frac{\chi_1}{\chi_2}}d(2V)^{\frac{\nu}{2}}}{\left(\frac{\chi_1}{\chi_2} + 2\sqrt{\frac{\chi_1}{\chi_2}}(2V)^{\frac{\nu}{2}} + \left[(2V)^{\frac{\nu}{2}}\right]^2\right)} \\ &= T\sqrt{\frac{\chi_1}{\chi_2}}\frac{1}{\sqrt{\frac{\chi_1}{\chi_2}} + (2V)^{\frac{\nu}{2}}}\Bigg|_{V(0)}^{V(t_V)} \\ &\le T\sqrt{\frac{\chi_1}{\chi_2}}\left(\frac{1}{\sqrt{\frac{\chi_1}{\chi_2}} + (2V(t_V))^{\frac{\nu}{2}}}\right) \\ &\le T. \end{aligned} \tag{19}$$

Equations (16) and (19) show that the system can be stable within the predefined time T.

Case $\frac{\chi_1}{\chi_2}-\left(\frac{\chi_3}{2\chi_2}\right)^2>0, \chi_3>2\sqrt{\chi_1\chi_2}$, the (16) can be expressed as (20). At the initial state $v(t)\to\infty$, and from (16), it can be derived that $v(t)\to 0$

$$\begin{aligned} t_V &= \int_{V(0)}^{V(t_V)} -\frac{Td(2V)^{\nu}}{B\chi_2\left[\left((2V)^{\frac{\nu}{2}}+\frac{\chi_3}{2\chi_2}\right)^2+\frac{\chi_1}{\chi_2}-\left(\frac{\chi_3}{2\chi_2}\right)^2\right]} \\ &= -\frac{T}{B\nu\chi_2\varsigma^{\frac{1}{2}}}\arctan\left[\varsigma^{-\frac{1}{2}}\wp_V(V)\right]\Bigg|_{V(0)}^{V(t_V)} \\ &\le \frac{T}{B\nu\chi_2\varsigma^{\frac{1}{2}}}\left[\frac{\pi}{2}-\arctan\left(\varsigma^{-\frac{1}{2}}\frac{\chi_3}{2\chi_2}\right)\right] \end{aligned} \tag{20}$$

where $\wp_V(V)=(2V)^{\nu}+\frac{\chi_3}{2\chi_2}$. It can be derived that $t_V\le T$. Therefore, the system states can achieve global stability within a predefined time T.

4) Discretization and Cost Function: By Euler discretizing (5) and (8), and then (21) and (22) can be obtained as

$$\begin{cases} e_1(k+1)=e_1(k)+T_s e_2(k) \\ e_2(k+1)=e_2(k)-aT_s u(k)+\Delta d_l(k) \end{cases} \tag{21}$$

$$\begin{cases} s_\omega(k)=e_2(k)+\frac{B}{T}\left(\chi_1\mathrm{sgn}^{1-\nu}(e_1(k))\right. \\ \qquad\qquad \left.+\chi_3 e_1(k)+\chi_2\mathrm{sgn}^{1+\nu}(e_1(k))\right) \\ s_\omega(k+1)=e_2(k+1)+\frac{B}{T}\left(\chi_1\mathrm{sgn}^{1-\nu}(e_1(k+1))\right. \\ \qquad\qquad \left.+\chi_3 e_1(k+1)+\chi_2\mathrm{sgn}^{1+\nu}(e_1(k+1))\right) \end{cases} \tag{22}$$

where $\Delta d_l(k)=d_l(k+1)-d_l(k)$, T_s is the discrete time period. Since the system states are not initially in the sliding state, an optimization approximation based on the target value zero (TVZ) of the sliding mode surface is explored in this article. The cost function based on TVZ is given as follows, and it is defined as the error between the predicted sliding mode face value and the tracking value

$$G(k)=s_\omega^2(k+1). \tag{23}$$

The optimized control gain $u(k)$, which makes the predictive sliding mode surface optimally approximate the target trajectory, can be obtained by solving $\partial G(k)/\partial u(k)=0$. Here, $u(k)$ represents the control output gain

$$\begin{aligned} &u(k) \\ &=\frac{1}{-aT_s}\begin{bmatrix}-e_2(k)+\Delta d_l(k)-A\left(\chi_1\mathrm{sgn}^{1-\nu}(e_1(k+1))\right.\\ -\left.\chi_3 e_1(k+1)-\chi_2\mathrm{sgn}^{1+\nu}(e_1(k+1))\right)\end{bmatrix}. \end{aligned} \tag{24}$$

The command of current control can be expressed as

$$i_{q\mathrm{ref}}(k)=i_q(k)+T_s u(k). \tag{25}$$

B. Predefined Time Fast Terminal Disturbance Observer

The sliding mode surface of the proposed predefined time fast terminal disturbance observer (PTFTDO) is defined as

$$\sigma=\omega_m-\hat{\omega}_m. \tag{26}$$

A linear item is introduced to speed up the convergence rate and improve the convergence performance. The proposed PTFTDO is designed as

$$\begin{aligned} \hat{d}_l =& -\frac{B_o}{T_o}\left(\chi_{o1}\mathrm{sgn}^{1-\nu}(\sigma)+\chi_{o3}\sigma+\chi_{o2}\mathrm{sgn}^{1+\nu}(\sigma)\right) \\ &-\int_0^t \chi_{o4}\mathrm{sign}(\sigma(t))\mathrm{d}\tau \end{aligned} \tag{27}$$

where χ_{o1}, χ_{o2}, $\chi_{o4}>0$, $0\le\chi_{o3}\le 2\sqrt{\chi_{o1}\chi_{o2}}$, T_o is the system state convergence time, and B_o is the tunning factor consisting of χ_{o1}, χ_{o2}, and χ_{o3}

$$\begin{cases} B_o=\begin{cases}\frac{1}{\rho\sqrt{\chi_{o1}\chi_{o2}}}, \chi_3=2\sqrt{\chi_{o1}\chi_{o2}} \\ \frac{1}{\rho\chi_{o2}\varsigma_o^{\frac{1}{2}}}\left[\frac{\pi}{2}-\arctan\left(\varsigma_o^{-\frac{1}{2}}\frac{\chi_{o3}}{2\chi_{o2}}\right)\right],\ \chi_{o3}>2\sqrt{\chi_{o1}\chi_{o2}}\end{cases}. \\ \varsigma_o=\frac{\chi_{o1}}{\chi_{o2}}-\left(\frac{\chi_{o3}}{2\chi_{o2}}\right)^2 \end{cases} \tag{28}$$

According to (3), it can be obtained that

$$\dot{\hat{\omega}}_m=ai_q-\hat{d}_l. \tag{29}$$

After differentiating (26), substituting (3), (27) and (29) yields

$$\begin{cases} \dot{\sigma}=-\frac{B_o}{T_o}\left(\chi_{o1}\mathrm{sgn}^{1-\nu}(\sigma)+\chi_{o3}\sigma+\chi_{o2}\mathrm{sgn}^{1+\nu}(\sigma)\right)+\iota \\ \dot{\iota}=-\chi_{o4}\mathrm{sign}(\sigma(t))+\dot{d}_l \end{cases}. \tag{30}$$

A Lyapunov function is chosen as $V_\sigma=\frac{1}{2}\sigma^2$, and the derivative of V_σ can be expressed as

$$\begin{aligned} \dot{V}_\sigma =& -\frac{B_o}{T_o}\left(\chi_{o1}\sigma^{2-\nu}+\chi_{o3}\sigma^2+\chi_{o2}\sigma^{2+\nu}\right) \\ &-|\sigma|\int\left(\chi_{o4}-\dot{d}_l\mathrm{sign}(\sigma)\right)dt\le 0 \end{aligned} \tag{31}$$

where $|\dot{d}_l|\le\phi$, $\phi\ge 0$. Let $\chi_{o4}\ge\phi$, and it is obvious that $|\sigma|\int(\chi_{o4}-\dot{d}_l\mathrm{sign}(\sigma))dt\ge 0$. Therefore, the proposed DO (30) is able to stabilize, and (31) can be derived as

$$\dot{V}_\sigma\le-\frac{B_o}{T_o}\left(2^{1-\frac{\nu}{2}}\chi_{o1}{V_\sigma}^{1-\frac{\nu}{2}}+2\chi_{o3}V_\sigma+2^{1+\frac{\nu}{2}}\chi_{o2}{V_\sigma}^{1+\frac{\nu}{2}}\right). \tag{32}$$

Then, the stability time T_{V_σ} for the estimated error from initial value $\sigma(0)$ to zero can be calculated by solving (32). Similar to the calculation process (16)–(20), it can be obtained that $T_{V_\sigma}\le T_o$, which shows that the designed DO can stabilize within a predefined time independent of the initial state.

The block diagram and flowchart of the proposed PTFTSMPC based on the PTFTDO (hereafter, PTFTSMPC refers to the PTFTSMPC based on the DO PTFTDO by default) are shown in Figs. 3 and 4, respectively.

IV. Simulation and Experimental Verification

The proposed PTFTSMPC speed controller shown in Fig. 3 is validated by simulations and experiments in this section.

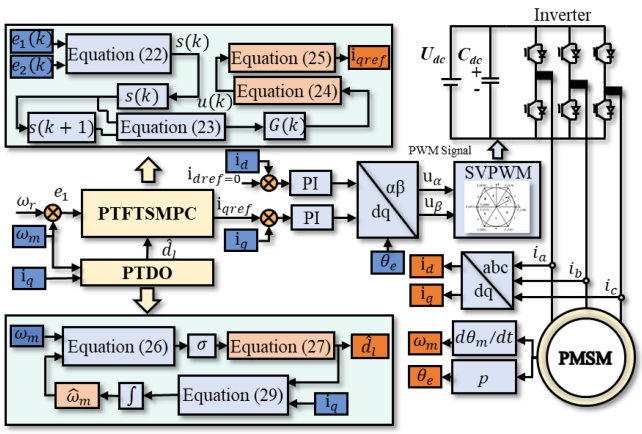

Fig. 3. Block diagram of the proposed PTFTSMPC.

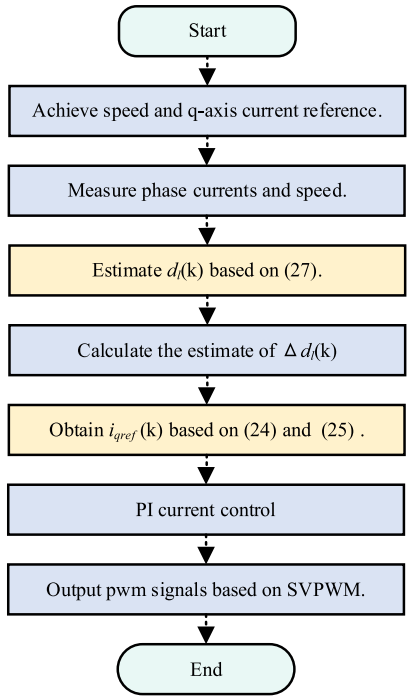

Fig. 4. Flowchart of the proposed PTFTSMPC.

A. Simulation Verification

To validate the effectiveness of the proposed PTFTSMPC speed controller, MATLAB/Simulink is utilized based on the block diagram in Fig. 3. i_{qref} is the output of the speed controller, and $i_{dref} = 0$ A. PI controllers are used in the current control, which are designed to be the same for all the speed controllers to ensure a fair comparison. The parameters of the SPMSM are given in Table I. The comparative experiments of the major speed control algorithms include: the traditional PI speed controller designed in [31] and [32], the conventional linear-sliding-mode-surface-based sliding mode predictive control (LSMPC) for speed regulation in [17] and [31], the proposed PTFTSMPC speed control method.

TABLE I
PARAMETERS OF THE SPMSM

Name	Parameters	Nominal Value
Stator Resistance	R_s (Ω)	0.3
Stator inductance	L (H)	4.6 x10^{-4}
Pole pairs	p	2
PM flux	Ψ_f (Vs)	0.0371
Rotor inertia	J (kg·m^2)	4.4109x10^{-5}
Rated speed	N (r/min)	3000
Rated power	P_r (W)	314
Rated torque	T_r (Nm)	1
DC link voltage	V_{dc} (V)	50

1) Parameter Tuning: Parameter Tuning of the Proposed Method: A small T_o of the PTFTDO represents fast convergence of the observer, but an excessively small T_o may cause jitter. To balance convergence rate and the observation jitter of the PTFTDO, the convergence time T_o is taken as 0.001 s in this article. Large values of χ_{o1}, χ_{o2}, and χ_{o3} will speed up the convergence time of the PTFTDO, but excessively large values may cause jitter. Although excessive χ_{o3} and χ_{o1} will also cause jitter, their impact is less significant compared to χ_{o2}. The values $\chi_{o1} = 3000$, $\chi_{o2} = 800$, $\chi_{o3} = 2500$ are set in simulations and experiments to minimize χ_{o2} under the condition of $T_o = 0.001$s. Additionally, $\chi_{o4} = 10^6$ is selected to satisfy the condition of $\chi_{o4} \geq \phi$. Based on the designed PTFTDO parameters, the PTFTSMPC parameters are selected by scanning the parameters grouping in Fig. 1. The steady-state error will increase with large ν and thus $\nu = 2/3$ is selected. Similar to the PTFTDO, large values of χ_1, χ_2, χ_3 will accelerate the speed convergence rate but may cause jitter. Thus, combined with the Fig. 1, parameter groups with T from 0.01 s to 0.045 s are scanned. Finally, the values $\chi_1 = 573.091$, $\chi_2 = 20.189$, and $\chi_3 = 177.889$ are taken for the PTFTSMPC speed controller in simulations and experiments.

Parameter Tuning of the LSMPC: The design of the LSMPC is same as that in [31]

$$\begin{cases} \mathrm{s}(k) = \mathrm{c}_1 e_1(k) + e_2(k) \\ u(k) = -\frac{1}{aT_s}\left(-c_1 e_1(k+1) - e_2(k) + s(k)\right. \\ \qquad \left. - k_1 s(k) - k_2 |s(k)|^{\nu} sign(s(k))\right) \\ i_{\mathrm{qref}}(k) = i_q(k) + T_s u(k) \end{cases} \tag{33}$$

where $c_1 > 0$, $0 < k_1 < 1$, $0 < k_2 < 1$. Large values of c_1, k_1 will accelerate the convergence rate of the system, but excessively large values may cause jitter. To be fair in comparison, $\mathrm{c}_1 = 200$, $k_1 = 0.7$, $k_2 = 0.6$, $\nu = 2/3$ are chosen in the simulations and experiments.

Parameter Tuning of the PI Speed Controller: According to [32], the output of the PI speed controller is $i_{qref} = (k_{p\omega} + k_{i\omega}/s)(\omega_r - \omega_m) - \omega_m B_a$, where B_a is the factor of the active damping and $B_a = (f_\omega J - b)/(1.5p\psi_f)$. The proportional coefficient $k_{p\omega}$ is designed as $k_{p\omega} = f_\omega J/(1.5p\psi_f)$, and the integration coefficient $k_{i\omega}$ is designed as $k_{i\omega} = f_\omega k_{p\omega}$. Here f_ω is the desired bandwidth of the PI speed controller and $f_\omega = 400$ rad/s. To balance the overshoot and dynamic response speed, $k_{p\omega} = 0.159$, $k_{i\omega} = 15.852$, and $B_a = 0.001$ are set in simulations and experiments.

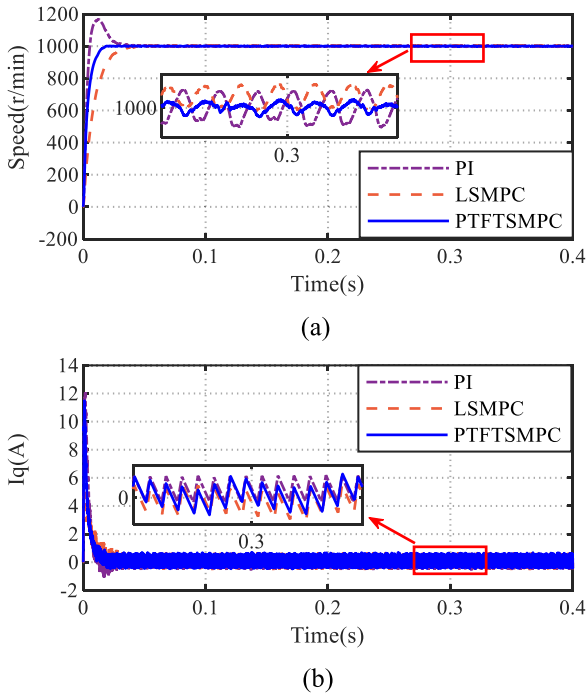

Fig. 5. Simulation results of speed and q-axis current for step response performance test. (a) Speed. (b) I_q.

Parameter Tuning of the PI Current Controllers: PI current controllers are implemented for the d-axis and q-axis current regulation. The parameters of the two PI current controllers are identical. From [33], the proportion factor k_{pc} and the integration factor k_{ic} of the PI current controllers are selected as $k_{pc} = f_c L$, $k_{ic} = f_c R_s$ and f_c is the bandwidth of the PI current controllers. To reduce the limitation of the current response rate on the speed dynamic performance, the bandwidth of the current controller is chosen as $f_c = 2\pi/(L/R_s) \approx 4100$ rad/s. After adjustment, the final factors are selected as $k_{pc} = 1.15$, $k_{ic} = 1231.995$ for simulations and experiments. For fair comparison, PI current controllers of the PI, LSMPC and PTFTSMPC are the same.

2) Step Response Performance: Fig. 5 shows the simulation results of the step response comparison with an amplitude of 1000 r/min at no load. The rise time of the PTFTSMPC is the 52.63% and 42.11% of that of the LSMPC. Besides the settling time of the PTFTSMPC is the 50.00% and 46.15% LSMPC. Despite the fact that the PI has shorter rise time, the settling time of the PI is 241.67% of that of the PTFTSMPC. Moreover, the overshoot of the PI is 16.60%, while the overshoot of the LSMPC and PTFTSMPC is approximately zero. Thus, the proposed PTFTSMPC exhibits superior dynamic response performance.

To further validate the superiority of the proposed method in dynamic response performance, a simulation with a sequence of different speed step commands response is conducted. A square wave command for speed is set as 200 r/min, 700 r/min, 1200 r/min, 1400 r/min at 0 s, 1 s, 2 s, and 3 s respectively. The frequency of the square wave speed command is 1 Hz and the duty cycle of the signal is 50%, 50%, 50%, and 40%, respectively. As shown in Fig. 6, the proposed method still has

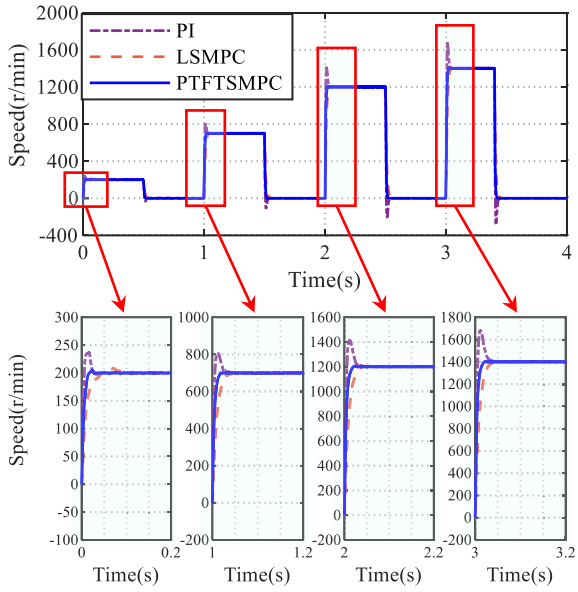

Fig. 6. Simulation results of a sequence of different speed step commands response performance.

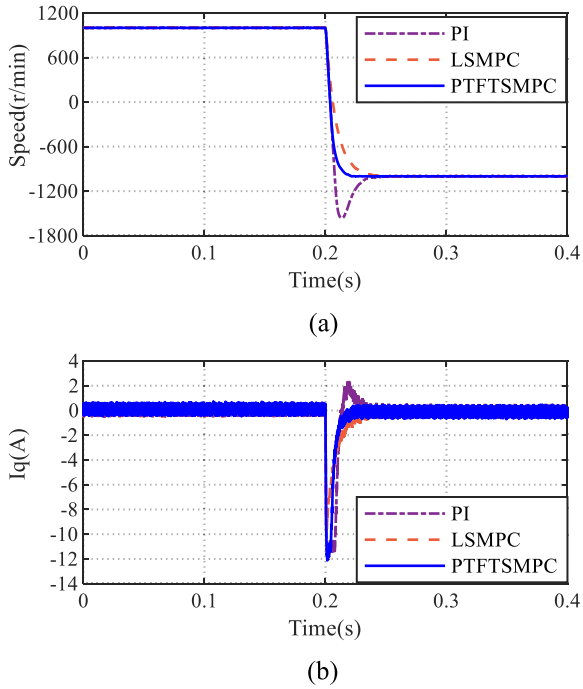

Fig. 7. Simulation results of speed and q-axis current for speed revisal performance test. (a) Speed. (b) I_q.

superior dynamic response performance compared to the PI and LSMPC with different speed step commands.

3) Speed Reversal Performance: As shown in Fig. 7, the speed reference of the SPMSM changes abruptly to -1000 r/min after running at 1000 r/min for 0.2 s without load. The proposed PTFTSMPC has a rise time close to that of the PI and a shorter settling time compared to both the PI and LSMPC. The undershoot of the PI is 28.07% while that of the LSMPC and PTFTSMPC is nearly zero. Therefore, the proposed

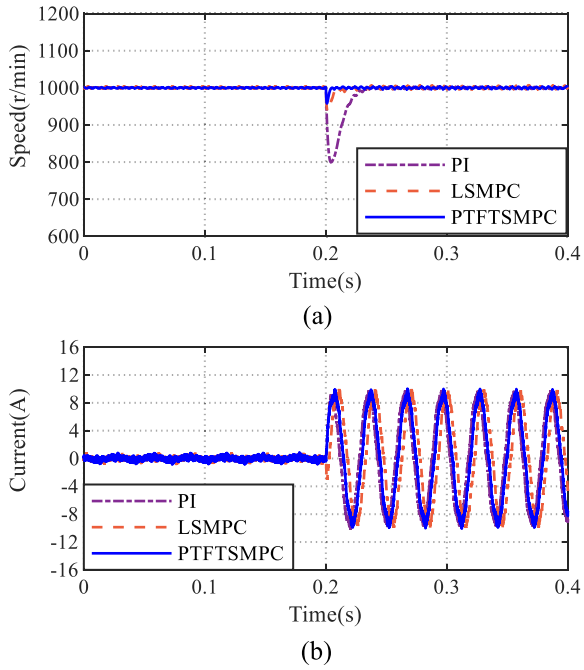

Fig. 8. Simulation results of speed and phase current for load disturbance performance test. (a) Speed. (b) Phase current.

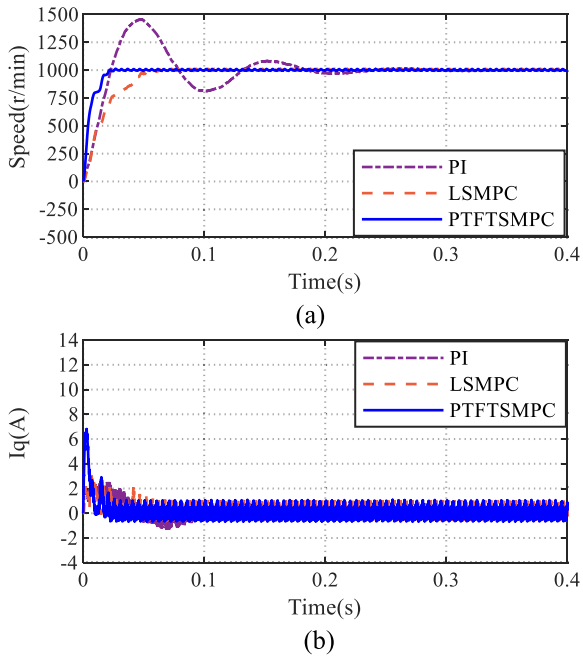

Fig. 9. Simulation results of speed and q-axis current for parameter mismatch test. (a) Speed. (b) I_q.

PTFTSMPC enhances the dynamic performance of the SPMSM speed control.

4) Load Disturbance Performance: As shown in Fig. 8, the SPMSM is running at 1000r/min without load, and a 1 N·m load torque is applied at 0.2 s. It can be observed that the overshoot of the proposed PTFTSMPC is 66.83% of the LSMPC and 21.00% of the PI. The overshoot recovery time of the PTFTSMPC is shorter than that of the PI and LSMPC. Hence, the PTFTSMPC demonstrates stronger antidisturbance capability.

5) Parameter Mismatch Test: Fig. 9 shows the simulation results of the parameter mismatch test performance comparison. The control parameter J is set to 10% of its real value, and the step response test is conducted with an amplitude of 1000 r/min. It is evident that the rise time and settling time of the proposed PTFTSMPC are shorter than those of the PI and LSMPC. The overshoot of the PI is 43.13% of the speed reference, which is the largest among the three. Thus, the proposed PTFTSMPC demonstrates stronger robustness against parameter mismatch compared to the PI and LSMPC.

B. Experimental Verification

The hardware platform consists of an SPMSM with a resolver, a load motor, a digital controller, a driver, and dc power supplies. As shown in Fig. 10, the algorithms are implemented on the digital controller based on TMS320F28335. The sample period is 0.0001 s, and the frequency of the inverter is set to 10 kHz. The signal from the SPMSM resolver is decoded by a 12-bit decoder board. The experimental platform framework is illustrated in Fig. 11. The control parameters of the PI, LSMPC and PTFTSMPC are the same as those used in the simulations, and d-axis current reference i_{dref} is set as 0 A. To ensure a fair

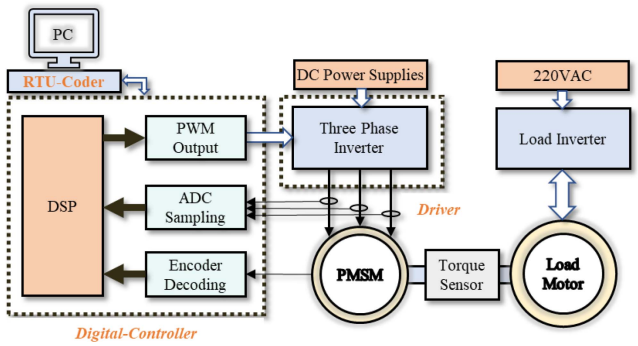

Fig. 10. Framework of the experimental platform.

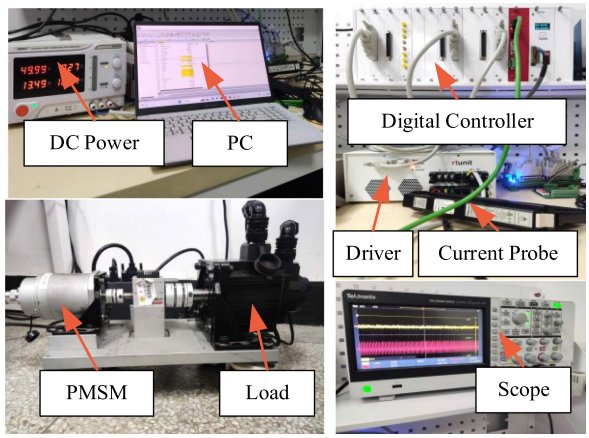

Fig. 11. Experimental setup.

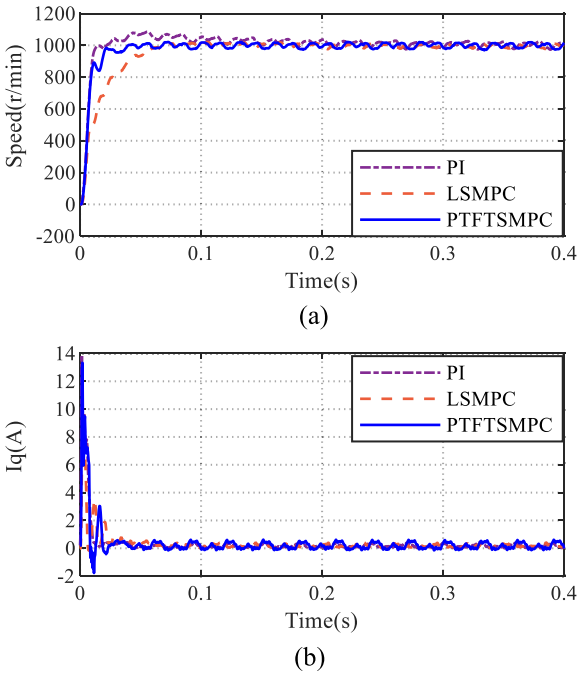

Fig. 12. Experiment results of speed and q-axis current for step response performance test. (a) Speed. (b) I_q.

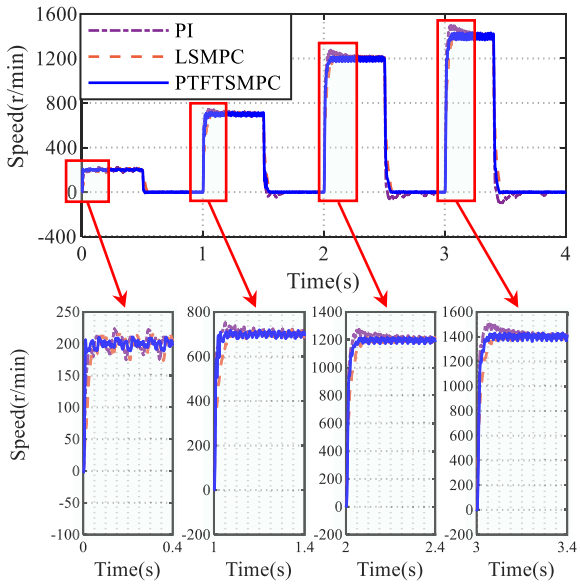

Fig. 13. Experiment results of a sequence of different speed step commands response performance.

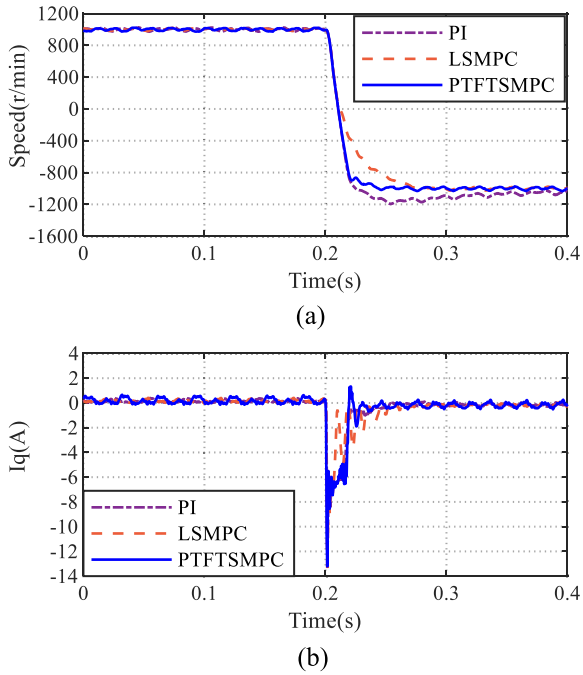

Fig. 14. Experiment results of speed and q-axis current for speed revisal performance test. (a) Speed. (b) I_q.

comparison, the same PI current controllers are applied in all the algorithms.

1) Step Response Performance: Fig. 12 compares the step response performance of the PI control, the conventional LSMPC and the proposed PTFTSMPC with an amplitude of 1000 r/min at no load. The proposed PTFTSMPC has a rise time close to that of the PI control and a shorter settling time compared to both the PI and LSMPC. The overshoot of PI is 8.518% of the speed reference while the overshoot of the other two control methods is nearly negligible. Overall, the proposed PTFTSMPC exhibits a faster convergence rate than the PI and LSMPC, indicating superior dynamic convergence performance.

In addition, Fig. 13 shows the experiment results of a sequence of different speed step commands response performance. A square wave command for speed is set as 200 r/min, 700 r/min, 1200 r/min, 1400 r/min at 0 s, 1 s, 2 s, and 3 s, respectively. The frequency of the square wave speed command is 1 Hz, and the duty cycle of the signal is 50%, 50%, 50%, and 40% respectively. The proposed method still exhibits superior dynamic response performance compared to the PI and LSMPC under different speed step commands.

2) Speed Reversal Performance: As shown in Fig. 14, the motor operates at 1000 r/min for 0.2 s without load initially, and the speed reference is abruptly changed to -1000 r/min. It is evident that the fall time and the settling time of the PTFTSMPC are shorter than those of the LSMPC. Although the PI has a short fall time, the settling times of the LSMPC and PTFTSMPC are 0.058 s and 0.029 s, respectively, which are 16.76% and 8.38% of the settling time of the PI. Additionally, the undershoot of PI is the 9.17% of the speed reference, which is the largest among all the algorithms. Clearly, the proposal PTFTSMPC displays better dynamic performance, particularly in terms of settling time.

3) Load Disturbance Performance: Fig. 15 shows the results of the antidisturbance capability comparison of the PI control, LSMPC and the proposed PTFTSMPC. The motor is subjected to a 1 N·m load torque after running at 1000 r/min without any load for 0.25 s. It can be observed that the PTFTSMPC has a lower overshoot than that of PI and LSMPC. The overshoot of the PTFTSMPC is the lowest, being 11.97% and 39.63% of that

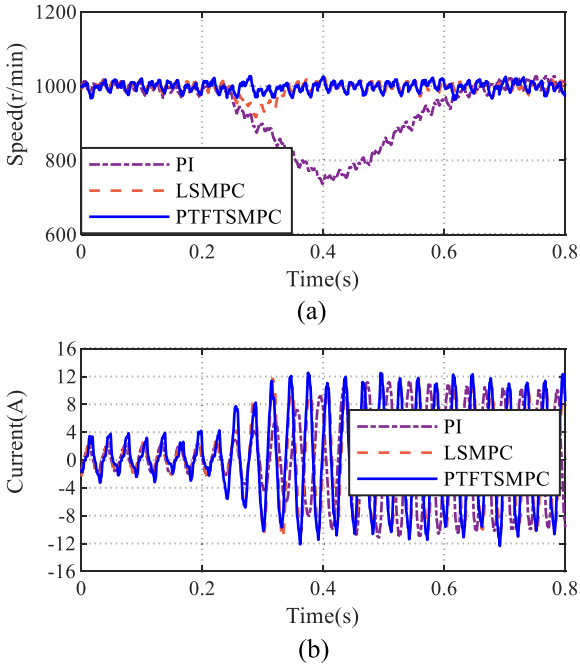

Fig. 15. Experiment results of speed and phase current for load disturbance performance test. (a) Speed. (b) Phase current.

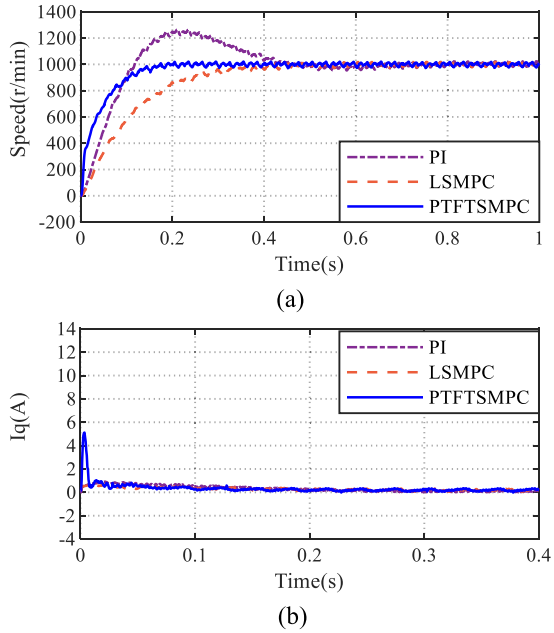

Fig. 16. Experiment results of speed and q-axis current for parameter mismatch test. (a) Speed. (b) I_q.

of the PI and LSMPC, respectively. Moreover, the recovery time of the PTFTSMPC is shorter than that of the PI and LSMPC. Hence, the proposal PTFTSMPC exhibits stronger antidisturbance capability than the PI and LSMPC.

4) Parameter Mismatch Test: The effect of ten-fold increase in ψ_f is equivalent to the ten-fold decrease in J. The comparison of the robustness to parameter mismatch is shown in Fig. 16. The

TABLE II
SIMULATION RESULTS

Tests	Parameters	PI	LSMPC	PTFTSMPC
Step response	Rise time/s (10%-90%)	0.004	0.019	0.008
	Settling time/s (50%-98%)	0.029	0.026	0.012
	Overshoot/%	16.60	/	/
Speed revisal	fall time/s (90%-10%)	0.007	0.025	0.012
	Settling time/s (50%-98%)	0.033	0.032	0.015
	Undershoot/%	28.07	/	/
Load disturbance	Undershoot /%	20.05	6.30	4.21
	Undershoot recovery time/s	0.037	0.013	0.005
Parameter variation	Rise time/s (10%-90%)	0.018	0.038	0.014
	Settling time/s (50%-98%)	0.068	0.04	0.017
	Overshoot/%	43.13	/	/

TABLE III
EXPERIMENTS RESULTS

Tests	Parameters	PI	LSMPC	PTFTSMPC
Step response	Rise time/s (10%-90%)	0.007	0.037	0.015
	Settling time/s (50%-98%)	0.090	0.051	0.015
	Overshoot/%	8.52	/	/
Speed revisal	fall time/s (90%-10%)	0.015	0.040	0.015
	Settling time/s (50%-98%)	0.346	0.058	0.029
	Undershoot/%	9.71	/	/
Load disturbance	Undershoot/%	26.31	8.37	3.15
	Undershoot recovery time/s	0.381	0.091	0.061
Parameter variation	Rise time/s (10%-90%)	0.085	0.213	0.105
	Settling time/s (50%-98%)	0.378	0.245	0.119
	Overshoot/%	26.46	/	/

control parameter J is set to 0.1 times its actual value, and a step response test with an amplitude 1000 r/min is employed. It is evident that the rise time of the proposed method is close to that of the PI and shorter than that of the LSMPC. In addition, the settling time of the PTFTSMPC is shorter than that of the PI and LSMPC. Therefore, it can be concluded that the PTFTSMPC also exhibits stronger robustness against parameter mismatch.

The specific results of the simulations and experiments are given in Tables II and III. The proposed PTFTSMPC demonstrates better dynamic response performance and stronger robustness against load disturbance and parameter variations in both simulations and experiments. The computational burden and the performance comparison of the proposed PTFTSMPC, LSMPC and PI are given in Tables IV and V. The proposed PTFTSMPC is recommended when the computational resources

TABLE IV
COMPUTATIONAL BURDEN OF THE PROPOSED METHOD AND OTHERS

Operations	PI	LSMPC	PTFTSMPC
+/-	4	10	20
*/÷	13	16	16
Program Time	4.61μs	6.46μs	13.61μs

TABLE V
COMPARISON OF THE PROPOSED METHOD AND OTHERS

Performances	PI	LSMPC	PTFTSMPC
Dynamic performance	medium	medium	good
External disturbances	poor	medium	good
Parameter sensitivities	poor	medium	good
Number of parameters	3	3	7
complexity	simple	medium	complex
Computational burden	low	medium	high

of the controller are sufficient and high control performance is required.

V. CONCLUSION

This article proposes a PTFTSMPC approach for SPMSM speed regulation, incorporating a predefined time DO to estimate and compensate for general disturbances. Theoretical analysis indicates that the proposed PTFTSLMS exhibits a faster convergence rate compared to LSLMS, FTSLMS, and PTSLMS. Stability analysis demonstrates that the system can be stabilized within a predefined time. Simulations and experiments are employed to validated that the proposed PTFTSMPC outperforms both PI and LSMPC in dynamic response and disturbance rejection. The proposed method significantly increases the dynamic response performance, load disturbance resistance and robustness to control parameter mismatch.

Future investigations will focus on combining adaptive algorithms with predefined time SMPC to reduce the workload of parameter tuning and improve the SPMC speed tracking accuracy.

REFERENCES

[1] K. Yu, S. Li, W. Zhu, and Z. Wang, "Sensorless control scheme for PMSM drive via generalized proportional integral observers and Kalman filter," *IEEE Trans. Power Electron.*, vol. 40, no. 3, pp. 4020–4033, Mar. 2025.

[2] G. Wu, S. Huang, Q. Wu, F. Rong, C. Zhang, and W. Liao, "Robust predictive torque control of N∗3-phase PMSM for high-power traction application," *IEEE Trans. Power Electron.*, vol. 35, no. 10, pp. 10799–10809, Oct. 2020.

[3] X. Zhang, Y. Cheng, Z. Zhao, and K. Yan, "Optimized model predictive control with dead-time voltage vector for PMSM drives," *IEEE Trans. Power Electron.*, vol. 36, no. 3, pp. 3149–3158, Mar. 2021.

[4] X. Liu, H. Yang, H. Lin, F. Yu, and Y. Yang, "A novel finite-set sliding-mode model-free predictive current control for PMSM drives without DC-link voltage sensor," *IEEE Trans. Power Electron.*, vol. 39, no. 1, pp. 320–331, Jan. 2024.

[5] Q. Li, H. Li, J. Gao, and R. Kennel, "Model predictive control using the singular perturbation theory for permanent-magnet synchronous machines," *IEEE Trans. Power Electron.*, vol. 39, no. 3, pp. 3533–3543, Mar. 2024.

[6] Z. Zhu, X. Wei, F. Yu, and Z. Zhang, "Overmodulatable parameter-free predictive current control for PMSMs," *IEEE Trans. Power Electron.*, vol. 40, no. 1, pp. 1774–1786, Jan. 2025.

[7] X. Liu et al., "Continuous control set predictive speed control of SPMSM drives with short prediction horizon," *IEEE Trans. Power Electron.*, vol. 37, no. 9, pp. 10166–10177, Sep. 2022.

[8] J. G. Cintron-Rivera, S. N. Foster, C. A. Nino-Baron, and E. G. Strangas, "High performance controllers for interior permanent magnet synchronous machines using look-up tables and curve-fitting methods," in *Proc. IEEE Int. Electron. Mach. Drives Conf.*, 2013, pp. 268–275.

[9] S. Hanke, S. Peitz, O. Wallscheid, J. Böcker, and M. Dellnitz, "Finite control-set model predictive control for a permanent magnet synchronous motor application with online least squares system identification," in *Proc. IEEE Int. Symp. Predictive Control Elect. Drives Power Electron.*, 2019, pp. 1–6.

[10] A. Brosch, S. Hanke, O. Wallscheid, and J. Böcker, "Data-driven recursive least squares estimation for model predictive current control of permanent magnet synchronous motors," *IEEE Trans. Power Electron.*, vol. 36, no. 2, pp. 2179–2190, Feb. 2021.

[11] X. Li et al., "Model-predictive control with parameter identification for multi-dual-active-bridge converters achieving accurate power balancing," *IEEE Trans. Power Electron.*, vol. 38, no. 9, pp. 10880–10894, Sep. 2023.

[12] F. Tinazzi, P. G. Carlet, S. Bolognani, and M. Zigliotto, "Motor parameter-free predictive current control of synchronous motors by recursive least-square self-commissioning model," *IEEE Trans. Ind. Electron.*, vol. 67, no. 11, pp. 9093–9100, Nov. 2020.

[13] X. An, G. Liu, Q. Chen, W. Zhao, and X. Song, "Adjustable model predictive control for IPMSM drives based on online stator inductance identification," *IEEE Trans. Ind. Electron.*, vol. 69, no. 4, pp. 3368–3381, Apr. 2022.

[14] J. Wang, F. Wang, Z. Zhang, S. Li, and J. Rodríguez, "Design and implementation of disturbance compensation-based enhanced robust finite control set predictive torque control for induction motor systems," *IEEE Trans. Ind. Electron.*, vol. 13, no. 5, pp. 2645–2656, Oct. 2017.

[15] S. Li, Y. Xu, W. Zhang, and J. Zou, "Robust deadbeat predictive direct speed control for PMSM with dual second-order sliding-mode disturbance observers and sensitivity analysis," *IEEE Trans. Power Electron.*, vol. 38, no. 7, pp. 8310–8326, Jul. 2023.

[16] X. Zhang, B. Hou, and Y. Mei, "Deadbeat predictive current control of permanent-magnet synchronous motors with stator current and disturbance observer," *IEEE Trans. Power Electron.*, vol. 32, no. 5, pp. 3818–3834, May 2017.

[17] L. He, F. Wang, and D. Ke, "FPGA-based sliding-mode predictive control for PMSM speed regulation system using an adaptive ultralocal model," *IEEE Trans. Power Electron.*, vol. 36, no. 5, pp. 5784–5793, May 2021.

[18] X. Lin, Y. Luo, Y. Gao, J. Liu, and L. Peretti, "A fixed-time convergence sliding mode observer based model-free predictive current control for PMSMs," in *Proc. IECON 49th Annu. Conf. IEEE Ind. Electron. Soc.*, Oct. 2023, pp. 1–5.

[19] M. Tian, T. Wang, Y. Yu, Q. Dong, B. Wang, and D. Xu, "Integrated observer-based terminal sliding-mode speed controller for PMSM drives considering multisource disturbances," *IEEE Trans. Power Electron.*, vol. 39, no. 7, pp. 7968–7979, Jul. 2024.

[20] J. Liu, M. Li, and E. Xie, "Noncascade structure equivalent SMC for PMSM driving based on improved ESO," *IEEE Trans. Power Electron.*, vol. 40, no. 1, pp. 611–624, Jan. 2025.

[21] Y. Chen and X. Liu, "A variable rate super-twisting sliding mode speed control with overcurrent protection for PMSM considering aperiodic and periodic disturbances," *IEEE Trans. Power Electron.*, vol. 40, no. 4, pp. 5787–5798, Apr. 2025, doi: 10.1109/TPEL.2024.3515086.

[22] Z. Tian, J. Yuan, X. Zhang, L. Kong, and J. Wang, "Modeling and sliding mode predictive control of the ultra-supercritical boiler-turbine system with uncertainties and input constraints," *ISA Trans.*, vol. 76, pp. 43–56, May 2018.

[23] S. Kang et al., "Discrete-time predictive sliding mode control for a constrained parallel micropositioning piezostage," *IEEE Trans. Syst. Man Cybern. -Syst.*, vol. 52, no. 5, pp. 3025–3036, May 2022.

[24] X. Lin et al., "Observer-based fixed-time control for permanent-magnet synchronous motors with parameter uncertainties," *IEEE Trans. Power Electron.*, vol. 38, no. 4, pp. 4335–4344, Apr. 2023.

[25] T. Zeng, X. Ren, and Y. Zhang, "Fixed-time sliding mode control and high-gain nonlinearity compensation for dual-motor driving system," *IEEE Trans. Ind. Electron.*, vol. 16, no. 6, pp. 4090–4098, Jun. 2020.

[26] B. Huang, F. Zhang, and P. Huang, "Predefined-time disturbance observer based predefined-time sliding mode control for space triangle tethered formation system," in *Proc. Int. Conf. Guid. Navigation Control*, 2022, pp. 1163–1173.

[27] M. Zhang, H. Zang, and L. Bai, "A new predefined-time sliding mode control scheme for synchronizing chaotic systems," *Chaos Solitons Fractals*, vol. 164, Nov. 2022, Art. no. 112745.
[28] L. He, F. Wang, J. Rodríguez, and M. L. Heldwein, "A robust predefined-time sliding mode predictive control for SPMSM speed regulation systems using an ultralocal model," *IEEE Trans. Ind. Electron.*, vol. 71, no. 8, pp. 8406–8415, Aug. 2024.
[29] J. D. Sanchez-Torres, D. Gomez-Gutierrez, E. Lopez, and A. G. Loukianov, "A class of predefined-time stable dynamical systems," *IMA J. Math. Control Inf.*, vol. 35, no. 1, pp. 1–29, 2018.
[30] W. Xu, A. K. Junejo, Y. Liu, M. G. Hussien, and J. Zhu, "An efficient antidisturbance sliding-mode speed control method for PMSM drive systems," *IEEE Trans. Power Electron.*, vol. 36, no. 6, pp. 6879–6891, Jun. 2021.
[31] D. Kong, H. Cai, and H. Zhai, "Double-layer fast terminal sliding mode predictive control for PMSM speed regulation," *IEEE Trans. Emerg. Sel. Topics Power Electron.*, vol. 12, no. 5, pp. 4876–4887, Oct. 2024.
[32] X. Zhang, Z. Wang, and H. Bai, "Sliding-mode-based deadbeat predictive current control for PMSM drives," *IEEE Trans. Emerg. Sel. Topics Power Electron.*, vol. 11, no. 1, pp. 962–969, Feb. 2023.
[33] S.-M. Yang and K.-W. Lin, "Automatic control loop tuning for permanent-magnet AC servo motor drives," *IEEE Trans. Ind. Electron.*, vol. 63, no. 3, pp. 1499–1506, Mar. 2016.

Delin Kong (Graduate Student Member, IEEE) was born in Xinyang, China. She received the B.S. degree in mechatronics engineering from Changzhou University, Changzhou, China, in 2018, and the M.S. degree in mechanical engineering from Harbin Institute of Technology, Harbin, China, in 2020. She is currently working toward the Ph.D. degree in electrical engineering with the School of Electrical Engineering, Southeast University, Nanjing, China.

From 2020 to 2023, she was an Engineer with Nanjing Chenguang Group Co. Ltd., Nanjing, China. Her research interests include sliding mode control and predictive control for electrical drives.

Haiwei Cai (Member, IEEE) received the B.S. degree from South China University of Technology, Guangzhou, China, in 2010, and the Ph.D. degree from The Ohio State University, Columbus, OH, USA, in 2015, both in electrical engineering.

From 2016 to 2018, he was an Application Engineer with ANSYS, Inc., Ann Arbor, MI, USA, where he focused on design and performance evaluation of electric machines for electrified vehicles. In 2018, he was with the School of Electrical Engineering, Southeast University, Nanjing, China, where he is currently as an Associate Professor. His research interests include design, analysis and control of electric machines for a wide range of applications such as vehicle electrification, renewable energy conversion and robotics.

Wenkai Zeng (Student Member, IEEE) was born in Fuzhou, China. He received the B.S. degree in electrical engineering from South China Agricultural University, Guangzhou, China, in 2023. He is currently working toward the M.S. degree in electrical engineering with the School of Electrical Engineering, Southeast University, Nanjing, China.

His research interests include torque ripple and parameter identification in electrical drives.